applied sciences

MDPI

Article

The Influence of Heat and Surface Treatment on the Functional Properties of Ti6Al4V Alloy Samples Obtained by Additive Technology for Applications in Personalized Implantology

Anita Kajzer, Gabriela Wielgus *, Krystian Drobina, Aleksandra Żurawska and Wojciech Kajzer

Department of Biomaterials and Medical Devices Engineering, Faculty of Biomedical Engineering, Silesian University of Technology, Roosevelta 40 Street, 41-800 Zabrze, Poland; anita.kajzer@polsl.pl (A.K.); kd304029@student.polsl.pl (K.D.); az306892@student.polsl.pl (A.Ż.); wojciech.kajzer@polsl.pl (W.K.)
* Correspondence: gabriela.wielgus@polsl.pl; Tel.: +48-(32)-277-74-51

Abstract

The main aim of this study was to evaluate the influence of heat and surface treatment on the physicochemical properties of samples produced using Direct Metal Sintering incremental technology from Ti64ELI titanium powder. Two groups of samples were selected for the study: sandblasted and mechanically polished samples. Each group consisted of samples in the initial state and after heat treatment carried out at temperatures of 800 °C, 910 °C, and 1020 °C. The article presents the results of microscopic metallographic observations, wettability and surface topography, hardness, and resistance to pitting corrosion in Ringer's solution, together with microscopic evaluation of the surfaces before and after testing. Based on the test results, both heat and surface treatments were found to alter the functional properties of the printed samples. All the tested samples show hydrophilic properties. Heat treatment at 1020 °C produces the best resistance to pitting corrosion. This information is important when selecting the mechanical properties of the biomaterial and the physicochemical properties of the surface for a specific type of stabilizer. The choice of appropriate heat treatment and surface treatment of the implant will also depend on the length of time the implant remains in the body.

Keywords: additive technology; Ti6Al4V alloy; heat treatment; grinding and mechanical polishing; personalized implants

check for updates

Academic Editors: Jakub Mesicek, Jana Petru, Jiří Hajnyš, Tomasz Kozior and Marek Pagáč

Received: 20 June 2025
Revised: 22 July 2025
Accepted: 23 July 2025
Published: 25 July 2025

Citation: Kajzer, A.; Wielgus, G.; Drobina, K.; Żurawska, A.; Kajzer, W. The Influence of Heat and Surface Treatment on the Functional Properties of Ti6Al4V Alloy Samples Obtained by Additive Technology for Applications in Personalized Implantology. *Appl. Sci.* **2025**, *15*, 8311. https://doi.org/10.3390/app15158311

Copyright: © 2025 by the authors. Licensee MDPI, Basel, Switzerland. This article is an open access article distributed under the terms and conditions of the Creative Commons Attribution (CC BY) license (https://creativecommons.org/licenses/by/4.0/).

1. Introduction

Devices used to promote bone fusion and stabilization, which come into direct contact with the human body environment, must meet a range of requirements adapted to their intended use and the individual needs of the patient [1]. The materials from which they are manufactured must be characterized by an appropriate set of mechanical properties and corrosion resistance in the tissue environment, which affects biocompatibility. Direct contact between the body and the device takes place through the surface of the device. This makes the surface structure of the device an important factor in determining its suitability for practical use. Among its characteristics, wettability, topography, and chemical composition are mainly considered. These parameters affect the application of the device, in particular its integration into bone [2–7].

Most often, titanium alloys are used for the manufacture of personalized implants, which are characterized by lightness, thanks to their low density (4.3–4.5 g/cm^3). The high strength, combined with the lightness, guarantees the durability of the device with the

right geometry and weight. The reduced modulus of elasticity of, for example, Ti6Al4V alloy ensures a good mechanical match to the properties of the bone, which supports its regeneration processes. Thanks to its very high corrosion resistance in the tissue environment, the material has very good biocompatibility. It is very important in view of its long residency in the body, which ensures appropriate stabilization and later recovery [8,9]. The development of design and manufacturing processes contributes to modern solutions in fracture stabilization and allows the creation of advanced implants, such as joint endoprostheses or dental implants, for example. These are most often manufactured using traditional methods [10,11].

Obtaining personalized implants by traditional methods is difficult, so they are being replaced by implants manufactured by additive methods. Examples of such technologies include selective melting of metal powders Selective Laser Melting (SLM) [12], Direct Metal Laser Sintering (DMLS), or laser beam melting (LBM). Powders of titanium alloys (e.g., Ti6Al4V ELI) are most used as the feedstock for DMLS or LBM printing [13,14]. With the help of CAD (Computer-Aided Design) and medical imaging methods such as CT (Computed Tomography) or MRI (Magnetic Resonance Imaging), it is possible to design an implant individually tailored to the patient's needs. Ti6Al4V ELI titanium alloy, due to its lower content of interstitial impurities, e.g., oxygen or nitrogen, is characterized by increased ductility and reduced alloy embrittlement compared to Ti6Al4V alloy. These properties are a result of reduced local stresses and the influence of dislocations in the material structure [15]. Ti6Al4V alloy powder is characterized by a spherical particle shape. This shape is obtained during the manufacturing process using the gas atomization method [16]. The particle shape provides good fluidity, which enables even layer distribution during printing, as well as a high application density. This translates into higher accuracy and uniformity of the manufactured products. Both parameters are important features in use for 3D printing technology. Particle sizes fall into two ranges, suitable for specific manufacturing methods. DMLS and EBM technologies use powder with gradations in the range 15–45 μm, while powder metallurgy and thermal spraying use powder with gradations between 45 μm–105 μm. The shape and distribution of Ti6Al4V powder particles are described in the literature [17–20]. The most important advantage of using DMLS technology is the ability to design and manufacture a perfectly shaped device. It will meet the patient's needs and material requirements, while maintaining its mechanical properties [21]. Desirable features for selecting the right material for the application are [22] density and porosity, particle size, conformal chemical composition, and morphological characteristics. Direct Metal Laser Sintering is mostly used for metal powders. Its characteristic feature in the process is the low laser power; the powder does not melt completely [23]. Heat treatment of the Ti6Al4V alloy is one of the processes that enables the microstructure and mechanical properties to be adapted to the requirements of medical applications. After the 3D printing process, it enables the transformation from the martensitic α' to the more stable $\alpha + \beta$ phases to be achieved [24]. Ti6Al4V is a biphasic $\alpha + \beta$ alloy, meaning that it contains two main crystalline phases: α and β. The combination of these two phases results in rarefied mechanical properties, which has led to its use particularly in the manufacture of orthopedic implants. The α phase is a hexagonal (A3) closely packed structure (hcp), while the β phase is regularly spatially centered (bcc). Heat treatment increases the inertness of the β phase, resulting in a change in the mechanical properties of the alloy [25,26].

It should be noted that the interaction of process parameters results in the formation of a regular lamellar structure and martensite decomposition. This has a significant effect on the mechanical and physical properties of the surface, which ensures that the surface of the additively manufactured implant interacts appropriately with the surrounding tissues.

An important objective of the research is to verify whether traditional surface modification methods, such as sandblasting or polishing, are equally important in the case of implants manufactured using powder technology, compared to traditional manufacturing methods [4].

Therefore, the aim of this study was to determine the effect of surface modification and heat treatment on the physicochemical properties of samples produced from Ti64 ELI alloy powder using DMLS technology. In particular, the surface topography, wettability, and pitting corrosion resistance were determined to observe whether surface modification improves the physicochemical properties of the material. In addition, metallographic microscopic examinations were carried out to analyze the internal structure of the material.

The results obtained will allow for the analysis of the physical and chemical properties of two groups of samples, which will make it possible to determine which surface treatment method is more advantageous. Currently, to manufacture orthopedic implants such as hip endoprostheses, a high-roughness stem is left in place for better osseointegration of the implant with the surrounding bone tissue. On the other hand, the surfaces of friction pairs (implant socket) should be characterized by low roughness in order to maintain appropriate tribological properties, as damage to friction pairs such as metal—polymer or metal–metal can lead to damage to the passive layer of the implant surface, which contributes to corrosion, e.g., pitting corrosion, the products of which, in the form of metal ions, are released into the surrounding tissues. This can lead to inflammation in the human body and even metallosis [4].

2. Materials and Methods

For the study, samples were printed from Ti6Al4V powder (EOS Titanium Ti64-Table 1) using DMLS additive manufacturing on an EOS M100 printer (EOS GmbH, Krailling Germany)—as shown in Figure 1. The particle size range for the initial powder used was 39 ± 3 µm. Each sample had two contours, 100% fill with the maximum laser beam power being 200 W, with parameters set at Ti64 20 µm FlexLine 1.x, a volume rate of 1.68 mm^3/s, and a layer thickness of 20 µm. Details of the process parameters are proprietary to EOS [17–20].

Table 1. Chemical composition of Ti64 powder-wt.-% [17].

O [%]	V [%]	Al [%]	Fe [%]	H [%]	C [%]	N [%]	Y [%]	Ti [%]
max 0.130	3.500–4.500	5.500–6.500	max 0.250	max 0.012	max 0.080	max 0.050	max 0.005	balance

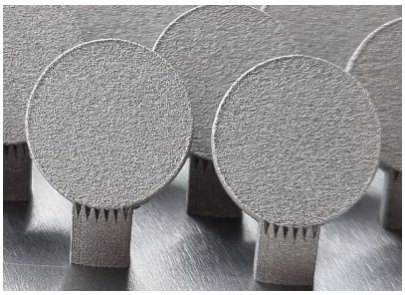


Figure 1. DMLS-printed samples with a diameter of 14 mm.

To remove the unmelted metal powder, the samples were sandblasted in a Renfert "VARIObasic" cabin sandblaster. Glass beads ranging from 90 µm to 150 µm fed through a nozzle at a pressure of 6 bar were used for the process. The samples were sandblasted for

120 s at an angle of 45 degrees. In turn, the heat treatment was then carried out in the high vacuum furnace "AMAZEMET inFURNER" with the following process parameters:

- The furnace was heated to 800 ± 10 °C, held the samples for 2 h, and was then tempered to 500 °C, followed by slow cooling to room temperature—as shown in Figure 2a;
- The furnace was heated to 910 ± 10 °C, held the samples for 2 h, and the samples were then cooled with the furnace to room temperature—as shown in Figure 2b.
- The furnace was heated to 1020 ± 10 °C, held the samples for 2 h, and the samples were then cooled with the furnace to room temperature—as shown in Figure 2c.

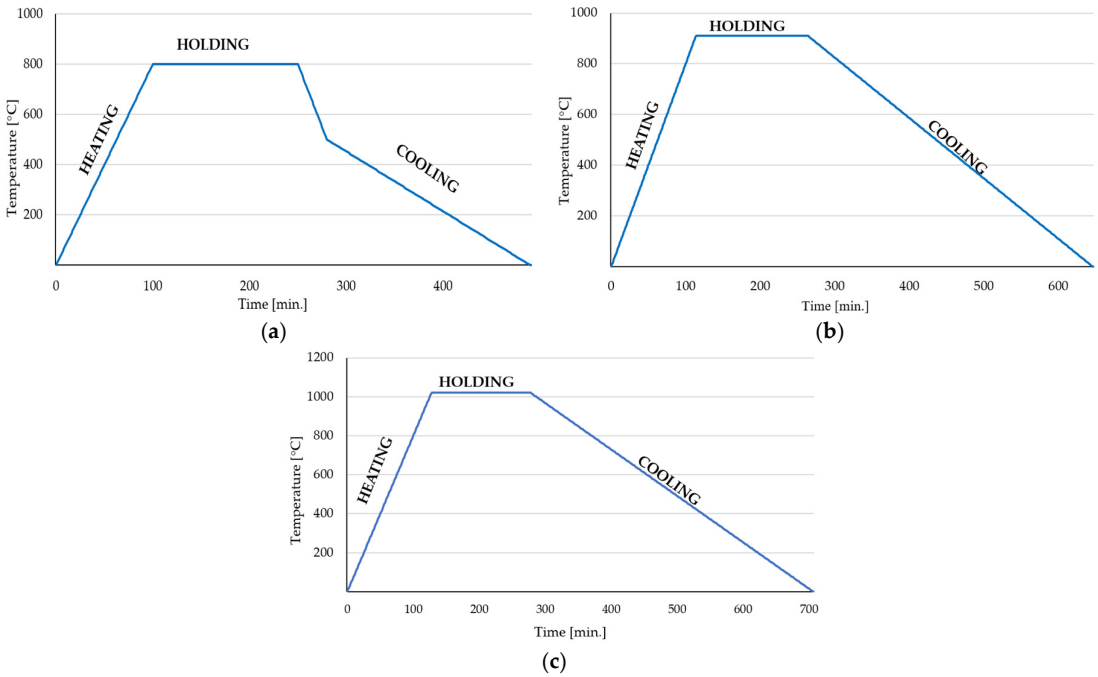


Figure 2. Heat treatment at: (**a**) 800 °C, (**b**) 910 °C, (**c**) 1020 °C.

All the samples were cleaned in a Struers Lavamin ultrasonic cleaner. Some of the samples were subjected to mechanical polishing on a Struers Tegramin-30 automatic grinder–polisher. For this purpose, the specimens were included in an automatic "Struers CitoPress-30" press in Struers' polypropylene resin with mineral and wood flour additives "Purifast" at a temperature of 150 °C, for a time of 3 min, and at a pressure of 250 bar. Subsequently, sanding was carried out on abrasive papers with gradations of P320, P800, and P1200 and mechanical polishing was carried out using an automatic sander–polisher Tegramin-30 from Struers with the following surface treatment parameters on a silicon oxide polishing cloth. The samples were divided into groups—as shown in Table 2.

Table 2. Division of samples for testing.

Group I	S	sandblasting—initial state
	S_800	sandblasting + heat treatment_800 °C
	S_910	sandblasting + heat treatment_910 °C
	S_1020	sandblasting + heat treatment_1020 °C
Group II	MP	mechanical polishing—initial state
	MP_800	mechanical polishing + heat treatment_800 °C
	MP_910	mechanical polishing + heat treatment_910 °C
	MP_1020	mechanical polishing + heat treatment_1020 °C

The tests were conducted on both the sandblasted and mechanically polished samples, as the type of surface preparation depends on the application of the implant. A highly developed surface is required for implants that require osseointegration, while a polished surface is required for short-term implants or those requiring low friction between components (e.g., knee joint) [2,27].

2.1. Material Structure

To reveal the structure of the test samples, microscopic metallographic examinations were carried out. For this purpose, the samples were included in the same way as in Section 2. The slides prepared in this way were etched in a solution of 10 mL hydrofluoric acid and 30 mL distilled water for 15 s. The final step involved observing the structure on a Leica DMi8 (Laica Microsystems, Wetzlar, Germany) optical microscope at 100× and 200× magnification.

2.2. Microscopic Observations

Surface topography was assessed using a scanning electron microscope (SEM) (TESCAN VEGA, Brno, Czech Republic) equipped with an SE detector operating at 10 keV energy and magnification of 2500×. Qualitative analysis of the chemical composition of the surface layer was performed using an EDS (Energy Dispersive Spectroscopy) detector.

2.3. Surface Roughness

The surface topography was assessed on a Leica Microsystems optical profilometer with the software "LeicaSCAN 6.6" and "Mountains Imaging Topography 10". This program generates reports with maps of the surface topography and a surface profile of the samples. From the data obtained, parameters such as Sa (complex surface profile roughness) were according to PN EN ISO 25178 1:2016 08 [28].

2.4. Wettability Test

Surface wettability measurements were carried out on a goniometer (BIOLIN Theta Flow, Gothenburg, Sweden) and assessed by measuring the contact angle value θ_{av}. Measurements were taken at room temperature, using distilled water. Three measurements were carried out on each sample with a drop of 1.5 µL. The measurement duration was one minute with a sampling frequency of 1 Hz. The results are presented tabularly and in the form of elemental spectra.

2.5. Pitting Corrosion Test

The pitting corrosion resistance test was carried out using the potentiodynamic method on a "VoltaLab PGP201" potentiostat (Radiometer, Villeurbanne Cedex, France) with VoltaMaster4 software, according to the recommendations of the PN-EN ISO 10993-15 standard [29]. The test stand consisted of a potentiostat and an electrochemical cell with the following electrodes: reference Ag/AgCl 3M KCl, auxiliary platinum electrode, and anode (test sample). Corrosion tests were started by determining the E_{ocp} (Open Circuit Potential) in currentless conditions, and then polarization curves were recorded. Polarization curves were recorded from the value of the initial potential $E_{start} = E_{ocp} - 100$ mV. After reaching the potential of E = 4 V, the polarization direction was changed. Based on the curves obtained using the Stern method, the corrosion potential E_{cor} [mV] and the value of polarization resistance R_p [kΩ·cm^2] were determined and current density I [mA/cm^2] by simple extrapolation of Tafel. The tests were carried out in a Ringer's solution at a temperature of 37 °C. Macroscopic observations of the surface of the samples before and after the corrosion resistance test were carried out using a digital microscope "Leica DVM6" at magnifications of 221×.

2.6. Hardness Test

The hardness test of the test specimens was carried out on a "Struers DuraScan" using a diamond pyramid with a square base, with a load of 49 N, as recommended by PN-EN ISO 6507-1:2007 [30]. Each successive specimen was subjected to five measurements on a single reference line.

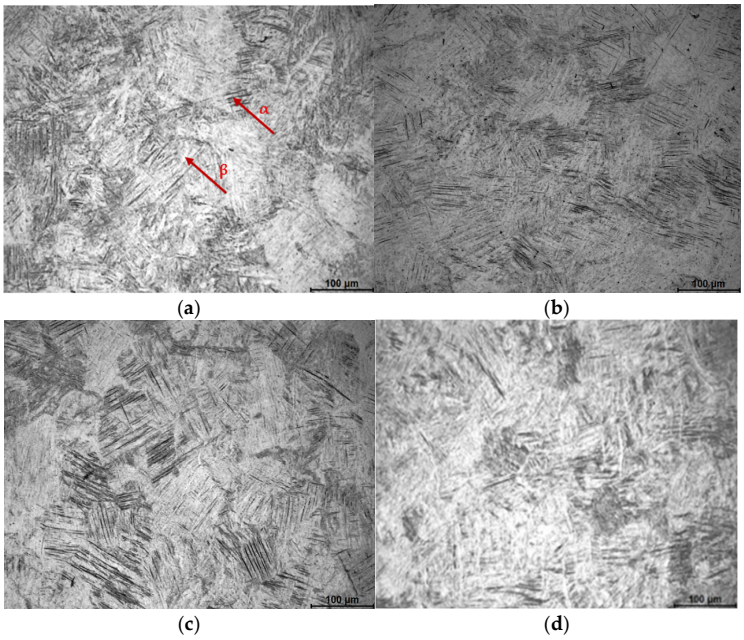
2.7. Statistical Analysis

Statistical analysis was performed as in a previous study: "The tests results are presented as a means with standard deviation. To determine the significance of differences for $p < 0.05$, the obtained results used a one-way and two-way analysis of variance (ANOVA). Statistically significant differences between groups were calculated using a one-way ANOVA followed by post-hoc Tukey test. To determine the homogeneity of variance, the Brown–Forsyth test was used. Statistical significance as before was declared at $p < 0.05$." [31].

3. Results

3.1. Material Structure

Based on the test results, the presence of a two-phase lamellar α + β structure was identified—as shown in Figure 3. The microstructure of the alloy after heat treatment at 1020 °C shows similarity to the microstructure of the material in the initial state. However, the α-phase is predominant in the initial state, whereas after heat treatment, a predominance of the structural phase β is observed. According to the literature [32], after heat treatment at 850 °C, the structure should consist of an α-phase matrix (gray areas) and an interlamellar β-phase (bright areas)—this is due to the different digestion rates of the phases. This phenomenon results from the different chemical compositions of each phase, which translate into their specific chemical and mechanical properties. These phases are clearly separated by phase boundaries, which allow for their unambiguous identification in the material structure [33]. It should also be emphasized that rapid cooling would result in the formation of a metastable α′ phase [34]. The biphasic α + β structure of printed Ti6Al4V alloy samples was also obtained by the authors of the publication [35], who carried out heat treatment at 850 °C for 2 h. According to the manufacturer's recommendations, for samples printed after heat treatment at 850 °C, the structure should consist of a matrix α phase (gray) and an interlayer β phase (light) [32].



(**a**) (**b**)

(**c**) (**d**)

Figure 3. Structure of Ti6Al4V alloy with initial state: (**a**), after heat treatment at: 800 °C (**b**), 920 °C (**c**), 1020 °C (**d**).

3.2. Microscopic Observations

From the SEM microscopic observation, there are differences between the analyzed surfaces of the samples after sandblasting and grinding together with mechanical polishing—as shown in Figure 4. Sandblasting is an essential step in the surface treatment of samples produced by powder technologies. Figure 4a shows the samples immediately after the 3D printing process, before sandblasting. On their surface, there is unmelted Ti6Al4V ELI powder, which must be removed prior to the next surface treatment step to prevent it from penetrating and accumulating in the surrounding tissues of the body, which can cause inflammation in the body. It can also cause increased friction between the components of the medical device's connection. The sandblasted-only surfaces show incompletely melted Ti6Al4V powder. In contrast, the polishing process provided a polished, smooth surface, which was confirmed during surface roughness tests.

The chemical analysis using EDS also showed no significant differences in the percentage of individual alloying elements in the composition of the samples. The approximate percentages of the individual elements are shown in Table 3.

Table 3. Approximate content [wt.-%] of elements.

Samples	Surface Layer Composition [wt.-%]				
	Ti	Al	V	Si	Other Elements
S	76.4	4.5	3.5	2.1	15.6
S_800	78.3	4.8	3.3	2.1	13.6
S_910	81.3	4.9	3.2	1.2	10.6
S_1020	77.1	4.7	2.7	2.6	15.5
MP	89.3	5.6	3.9	-	1.2
MP_800	89.8	5.5	3.8	-	0.9
MP_910	89.3	5.5	3.9	-	1.3
MP_1020	89.8	5.6	3.8	-	0.8

The elements included in the Ti6Al4V alloy were identified. The occurrence of silicon during the analysis indicates residues from the sandblasting process. The heat treatment process did not clearly affect the changes in the chemical composition. The higher contents of Ti and Al are due to the reagents used during the surface polishing process of the samples.

According to the recommendation of the standard EOS Titanium Ti64 Grade 23—Material Data Sheet, Metal Solutions [17], the Al content should be between 5.5 and 6.5. The values obtained for the polished surfaces are within this range (5.5–5.6). The presence of Si impurities on the surface resulting from the sandblasting process may constitute a barrier and lead to lower values of the analyzed elements using the qualitative EDS method.

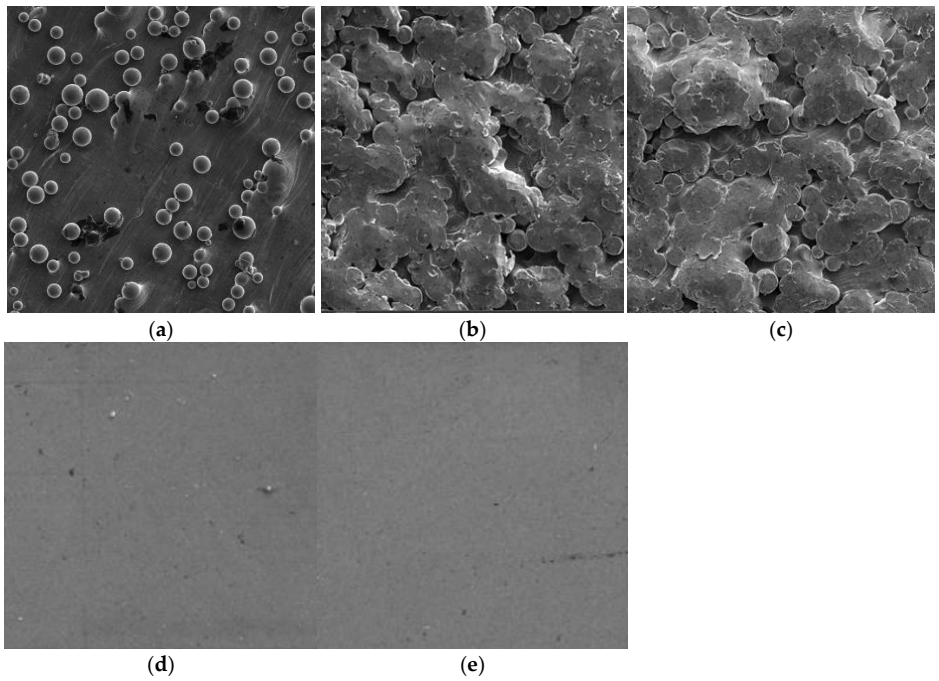


Figure 4. Example of surface samples for group I and II samples (SEM): (**a**) initial state, (**b**) S, (**c**) S_910–mag. 500×, (**d**) MP, (**e**) MP_910–mag. 1500×, det SE, energy 10 keV.

3.3. Surface Roughness

Examples of the surface roughness test results are shown in Figures 5 and 6.

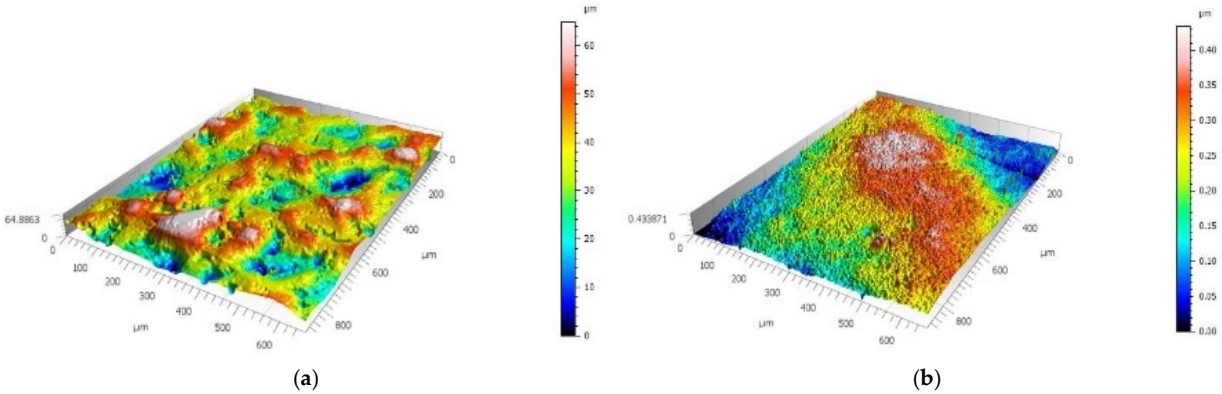


Figure 5. Examples of maps of the surface topography samples: (**a**) S, (**b**) MP.

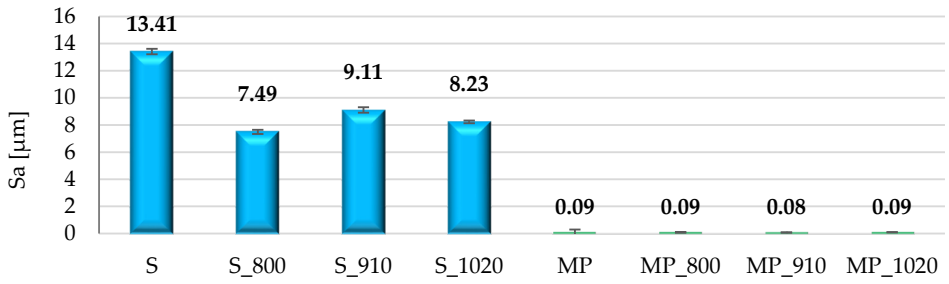


Figure 6. Comparison of the Sa parameter.

Mechanical surface polishing resulted in a significant reduction in surface roughness with respect to the surface after sandblasting regardless of the heat treatment temperature used, which was also confirmed by statistical ANOVA analysis ($p < 0.05$). No significant differences in the Sa parameter were observed between the individual surfaces of the samples in this group ($p > 0.05$). However, in the group of sandblasted specimens, the lower surface roughness after heat treatment may result from excessive melting of metal powder grains at high temperatures, leading to partial filling of the pores created during 3D printing [2]. For printed surfaces after heat treatment at 850 °C and before sandblasting according to the manufacturer's recommendations, the roughness should be 8.4 to 9.0 µm.

3.4. Wettability Test

Examples of droplets obtained during contact angle determination are shown in Figure 7.

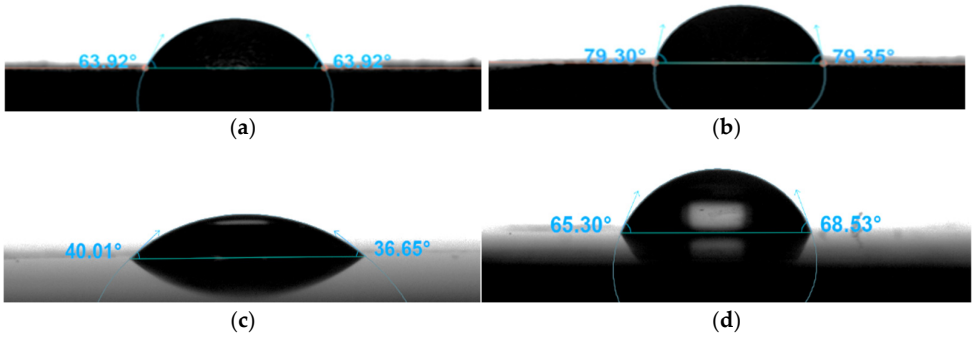


Figure 7. Determination of contact angles: (**a**) initial state—after sandblasting, (**b**) condition after treatment at 800 °C—after sandblasting, (**c**) initial condition—after polishing, (**d**) condition after treatment at 800 °C—after polishing.

Based on the results obtained for the mean contact angle value, it was observed that the samples in groups one and two have hydrophilic properties—as shown in Figure 8.

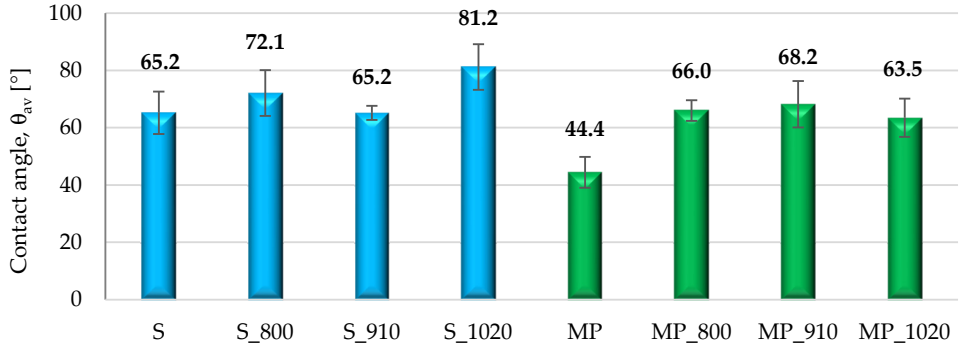


Figure 8. Mean values of contact angle θ_{av}.

The surfaces after mechanical polishing are characterized by higher wettability. It can also be observed that the wettability of the samples in the initial state shows the greatest reduction in the contact angle value in relation to the surfaces after sandblasting. Tests carried out by the authors [36] indicate that the contact angle values for samples with sandblasted surfaces ranged from 75.78 ± 2.26° to 92.82 ± 3.14°. For this study, the increase in contact angle was dependent on the laser power of the incremental printing process. The authors of publication [37], in contrast, indicate the hydrophilicity of all the samples made using additive technology. The mean value of the θ_{av} angle was 63.81 ± 7.55°.

3.5. Pitting Corrosion Test

The polarization curves for two groups of samples are presented in Figure 9. Differences in pitting corrosion resistance were found between the tested groups of samples—as shown in Table 4. Samples after mechanical polishing had higher corrosion resistance. In the case of samples after sandblasting, heat treatment at 1020 °C resulted in a decrease in corrosion potential and an increase in polarization resistance, which is confirmed by the authors' research [38].

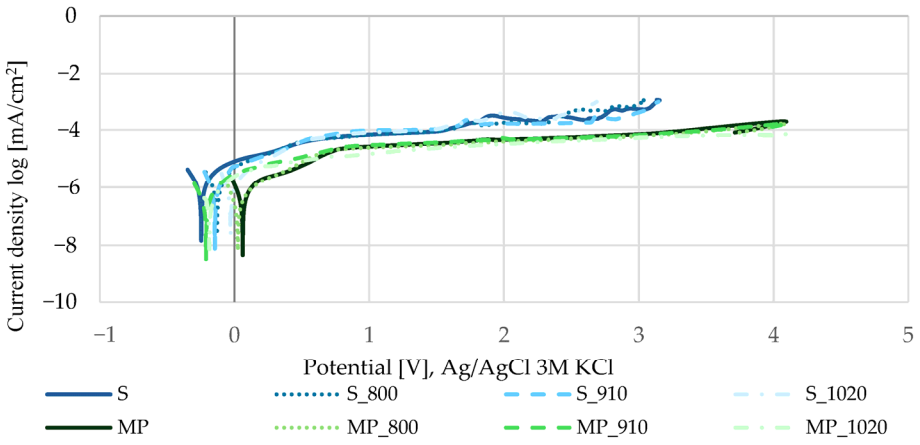


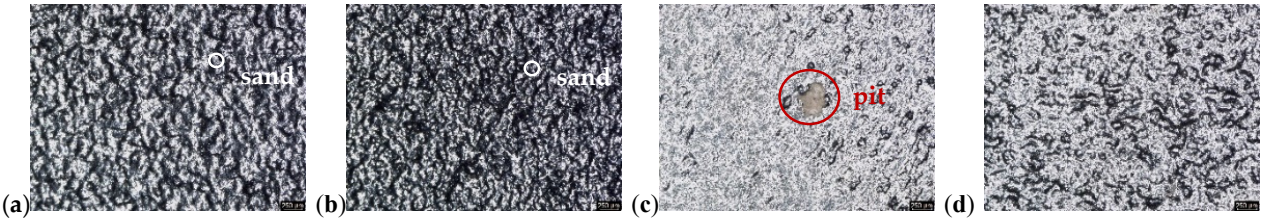
Figure 9. Polarization curves in logarithmic form for samples from two groups.

Table 4. Pitting corrosion resistance results for samples from groups I and II.

Samples	I [mA/cm ^{2}]	E_{cor} [mV]	R_p [kΩ·cm ^{2}]
S	818 ± 139	−226 ± 87	29 ± 1.5
S_800	940 ± 487	−115 ± 30	32 ± 0.1
S_910	766 ± 145	−118 ± 6.4	31 ± 0.9
S_1020	164 ± 79	−51 ± 54	89 ± 29
MP	215 ± 116	−58 ± 16	95 ± 43
MP_800	289 ± 69	−63 ± 133	95 ± 32
MP_910	615 ± 88	−233 ± 45	63 ± 48
MP_1020	150 ± 53	−207 ± 66	67 ± 17

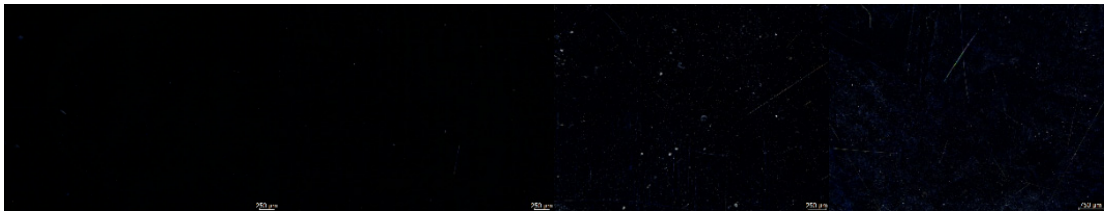
The greatest resistance to pitting corrosion for sandblasted specimens is characterized by the specimens after heat treatment at 1020 °C. The lowest current density and the highest values of corrosion potential and polarization resistance were determined for this group. To confirm the results of the pitting corrosion resistance test, macroscopic observations of the surface of the samples were carried out at 221 × magnification—as show in Figures 10 and 11. Few pits were found on the surfaces of sandblasted specimens (Figure 10c) for specimens

with less resistance to this type of corrosion. This is confirmed by the results obtained by the authors [38], who found pits on the surface after testing for pitting corrosion resistance. The number was smaller for heat-treated samples [39].



(**a**) (**b**) (**c**) (**d**)

Figure 10. Surface of samples before (**a**,**b**) and after (**c**,**d**) corrosion resistance test (group I): (**a**) S, (**b**) S _1020, (**c**) S, (**d**) S_1020, mag. 221×, bar scales 250 µm.



(**a**) (**b**) (**c**) (**d**)

Figure 11. Surface of samples before and after corrosion resistance test (group II): (**a**) MP, (**b**) MP_1020, (**c**) MP, (**d**) MP_1020 mag. 221×, bar scales 250 µm.

In the case of the group I samples, sand grains on the surface of the test material can also be observed. On the other hand, the black images obtained (for the second group of samples) are related to the polished surface of the sample. Mechanical polishing provides a high degree of surface smoothness, significantly increasing its ability to reflect light bidirectionally. The appearance of scratches on the surface of the samples after testing for resistance to pitting corrosion is the result of placing them in an electrochemical cell. The pitting observed occurs only in the case of sample "S". According to standard [29] if a material exhibits corrosion resistance up to 2 V, it can be considered corrosion-resistant across the entire measurement range.

3.6. Hardness Test

The results of the hardness measurements are shown in Figure 12.

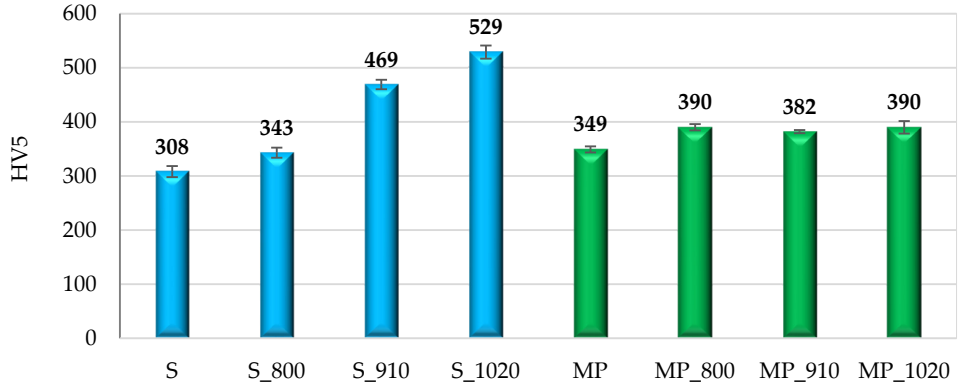


Figure 12. Results of hardness test for two research groups.

Differences in values were found depending on the surface preparation method. Heat treatment has a significant effect on the hardness of Ti6Al4V alloy, especially for materials

produced by DMLS. The post-treatment hardness can be increased depending on the heat treatment parameters used. For the test specimens after sandblasting, varying hardness values were observed depending on the process used: approximately 343 HV when annealed at 800 °C, 469 HV at 910 °C, and an increase to 529 HV ($p < 0.05$) at 1020 °C, which is explained by a change in dislocation density and grain boundary distribution [35].The authors of publication [35] also observed that despite the same microstructure of the samples at temperatures (950 °C and 1000 °C), they confirmed a difference in hardness, which may be caused by grain formation, as well as its size, thickening, or fragmentation. These properties affect characteristics such as strength and hardness.

For printed surfaces after heat treatment at 850 °C and before sandblasting according to the manufacturer's recommendations, the hardness should be between 344 HV and 346 HV [32]. On the other hand, comparable hardness was obtained for samples after mechanical polishing in the initial state and sandblasted samples heat-treated at 800 °C. For the other polished sample variants, comparable hardness values were obtained ($p > 0.05$).

4. Discussion of Results and Conclusions

Ti6Al4V alloy, after 316LVM steel, is the most used biomaterial for implants in orthopedics. Amongst others, bone plates, stabilizing screws, and endoprostheses are made from this alloy. The development of additive manufacturing technologies makes it possible to implement modern design solutions and personalize implants, even with complex shapes. For this reason, performance tests were carried out for two groups of specimens prepared accordingly, with the aim of comparing the surface preparation and heat treatment applied. It was found that both the surface modification and the heat treatment influenced the properties of the samples produced by the incremental method in Ti6Al4V alloy. Based on metallographic microscopic studies, a biphasic $\alpha + \beta$ structure was found for all the samples studied. The post-treatment method influenced the surface roughness values. The highest value of the Sa parameter was determined for the surface of sandblasted samples in the initial state—13.41 µm—while the heat treatment influenced the decrease in roughness in this group of samples—0.09 ± 0.01 µm. The lowest roughness was found for the surfaces after mechanical polishing, regardless of the temperature of the heat treatment applied. Additional surface analysis using a scanning electron microscope revealed unmelted titanium alloy powder, as well as sand grains after the sandblasting process, which was confirmed by qualitative analysis of the chemical composition using an EDS detector. Mechanical polishing removes the unmelted powder and sand residues after the sandblasting process. Hydrophilic properties were found for all the surfaces analyzed from 44.4° to 81.2°. A material is assumed to have hydrophilic properties when the value of the contact angle is between 0° and 90°. The hydrophilicity of the Ti6Al4V alloy promotes cell adhesion to its surface, which is an important aspect in the context of implant applications, especially in orthopedics. The surface layer of the material should provide adequate adsorption properties for proteins and promote their functionality, including cell proliferation [40,41]. Heat treatment causes an increase in the contact angle and thus a decrease in wettability. Considering the tissue environment, the resistance of the implant to pitting corrosion is important. Of the sample groups analyzed, all the mechanically polished samples show the greatest resistance to this type of corrosion. This was also confirmed by macroscopic observations of the surface after testing. For this group, a smaller effect of heat treatment on the change in hardness was also found (from 382 HV5 to 390 HV5).

In summary, an innovative approach described in the paper is the use of additive technologies, which replace traditional implant manufacturing methods with modern solutions with a higher degree of personalization. The original research aims to demonstrate how

different heat treatment temperatures and surface treatments affect the physicochemical properties of printed Ti6Al4V by using the DMLS method.

It can be concluded that the selection of the type of surface and heat treatment will depend on the application of the implant in the tissue environment. Sandblasting is an important step after the 3D printing process to remove unbound powder particles from the sample surface. Skipping sandblasting could result in the presence of unintegrated Ti64 ELI alloy powder grains on the surface, which would significantly affect morphology evaluation. The use of mechanical polishing contributes to reducing surface roughness, which improves also resistance to pitting corrosion. A potential disadvantage of mechanical polishing is too smooth a surface, which can limit cell adhesion and hinder the process of osseointegration, which is crucial for connecting the implant with the surrounding bone. Implants that are removed from the body after the stabilization process are required to have low surface roughness in addition to appropriate mechanical properties and biocompatibility. This contrasts with long-term implants (e.g., endoprostheses), for which the surface should be porous, which promotes osteointegration.

Subsequent work will focus on the surfaces of samples obtained by the additive method but subjected to surface functionalization. The layers produced will aim, for example, to increase the surface hardness and abrasion resistance of multi-element stabilizers, the components of which undergo a frictional process during use.

Author Contributions: Conceptualization, A.K. and W.K.; Formal analysis, A.K. and W.K. Methodology, A.K. and G.W.; Founding acquisition A.K. and W.K., Resources, G.W.; Writing—original draft, A.K., G.W., K.D., A.Ż. and W.K. All authors have read and agreed to the published version of the manuscript.

Funding: This research received no external funding.

Institutional Review Board Statement: Not applicable.

Informed Consent Statement: Not applicable.

Data Availability Statement: The original contributions presented in the study are included in the article, further inquiries can be directed to the corresponding author.

Acknowledgments: The Article Processing Charge was financed under the European Funds for Silesia 2021–2027 Program co-financed by the Just Transition Fund—project entitled "Development of the Silesian biomedical engineering potential in the face of the challenges of the digital and green economy (BioMeDiG)". Project number: FESL.10.25-IZ.01-07G5/23.

Conflicts of Interest: The authors declare no conflict of interest.

References

1. Marin, E.; Lanzutti, A. Biomedical Applications of Titanium Alloys: A Comprehensive Review. *Materials* **2024**, *17*, 114. [CrossRef] [PubMed]
2. Kajzer, W.; Wielgus, G.; Kajzer, A. Mechanical and Physicochemical Properties of Ti6Al4V Alloy After Plastic Working and 3D Printing Intended for Orthopedics Implants. *Appl. Sci.* **2024**, *14*, 11181. [CrossRef]
3. Orłowska, A.; Kajzer, W.; Goldsztajn, K.; Gawron, A.; Godzierz, M.; Nowińska, K.; Basiaga, M.; Simka, W.; Szewczenko, J. Functionalization of 3D printed Ti6Al4V high-porous spinal implant surface with use of plasma electrolytic oxidation. *Appl. Surf. Sci.* **2024**, *659*, 159948. [CrossRef]
4. Orłowska, A.; Szewczenko, J.; Kajzer, W.; Goldsztajn, K.; Basiaga, M. Study of the Effect of Anodic Oxidation on the Corrosion Properties of the Ti6Al4V Implant Produced from SLM. *J. Funct. Biomater.* **2023**, *14*, 191. [CrossRef] [PubMed]
5. Firdaus, M.N.; Verlieza, Z.; Buwana, D.S.; Rachmadi, B.T.; Soetojo, B.W.; Desnantyo, A.T. Future of orthopaedic in bone defect by using 3D-printed personalized implants: A systematic review. *J. Assoc. Med. Sci.* **2025**, *58*, 234–242. [CrossRef]
6. Cong, B.; Zhang, H. Innovative 3D printing technologies and advanced materials revolutionizing orthopedic surgery: Current applications and future directions. *Front. Bioeng. Biotechnol.* **2025**, *13*, 1542179. [CrossRef] [PubMed]

7. Ling, K.; Wang, W.; Liu, J. Current developments in 3D printing technology for orthopedic trauma: A review. *Medicine* **2025**, *104*, e41946. [CrossRef] [PubMed]
8. Goldsztajn, K.; Godzierz, M.; Hercog, A.; Władowski, M.; Jaworska, J.; Jelonek, K.; Woźniak, A.; Kajzer, W.; Orłowska, A.; Szewczenko, J. Properties of biodegradable polymer coatings with hydroxyapatite on a titanium alloy substrate. *Acta Bioeng. Biomech.* **2024**, *26*, 121–132. [CrossRef] [PubMed]
9. Lisoń-Kubica, J.; Taratuta, A.; Goldsztajn, K.; Antonowicz, M.; Walke, W.; Dyner, A.; Basiaga, M. Modern methods of surface modification for new-generation titanium alloys. *Acta Bioeng. Biomech.* **2022**, *24*, 147–158. [CrossRef] [PubMed]
10. Warreth, A.; Ibieyou, N.; O'Leary, R.B.; Cremonese, M.; Abdulrahim, M. Dental implants: An overview. *Implant. Dent.* **2017**, *44*, 596–620. [CrossRef]
11. Guo, L.; Naghavi, S.A.; Wang, Z.; Varma, S.N.; Han, Z.; Yao, Z.; Wang, L.; Wang, L.; Liu, C. On the design evolution of hip implants: A review. *Mater. Des.* **2022**, *216*, 110552. [CrossRef]
12. Kiel-Jamrozik, M.; Jamrozik, W.; Witkowska, I. The heat treatment influence on the structure and mechanical properties of Ti6Al4V alloy manufactured by SLM technology. *Innov. Biomed. Eng.* **2017**, *623*, 319–327. [CrossRef]
13. Chang, J.Z.-C.; Tsai, P.-I.; Kuo, M.Y.-P.; Sun, J.-S.; Chen, S.-Y.; Shen, H.-H. Augmentation of DMLS Biomimetic Dental Implants with Weight-Bearing Strut to Balance of Biologic and Mechanical Demands: From Bench to Animal. *Taiwan. Mater.* **2019**, *12*, 164. [CrossRef] [PubMed]
14. Orłowska, A.; Szewczenko, J.; Kajzer, W.; Goldsztajn, K.; Basiaga, M. Influence of anodic oxidation on the biocompatibility of Ti6Al4V implants made by the SLM method. In Proceedings of the 32nd Annual Conference of the European Society for Biomaterials, Bordeaux, France, 4–8 September 2022; p. 223.
15. Available online: https://gsalloy.com/pl/ti6al4v-vs-ti6al4v-eli-a-comprehensive-comparison/ (accessed on 26 April 2025).
16. Campos, F.d.O.; Araujo, A.C.; Munhoz, A.L.J.; Kapoor, S.G. The influence of additive manufacturing on the micromilling machinability of Ti6Al4V: A comparison of SLM and commercial workpieces. *J. Manuf. Process.* **2020**, *60*, 299–307. [CrossRef]
17. EOS GmbH-Electro Optical Systems: Krailling/Munich Germany. Available online: https://www.eos.info (accessed on 19 June 2025).
18. *EOSTitaniumTi64 for EOS M300-4*; Material Data Sheet. EOS GmbH—Electro Optical Systems: Krailling, Germany, 2022.
19. *Instruction EOS M 100*; User Manual EOS M100; EOS GmbH—Electro Optical Systems: Krailling, Germany, 2019.
20. *EOSM100*; Parameter Sheet. EOS GmbH—Electro Optical Systems: Krailling, Germany, 2015.
21. Gogolewski, D.; Kozior, T.; Zmarzły, P.; Mathia, T.G. Morphology of Models Manufactured by SLM Technology and the Ti6Al4V Titanium Alloy Designed for Medical Applications. *Materials* **2021**, *14*, 6249. [CrossRef] [PubMed]
22. Liu, Z.; Zhao, D.; Wang, P.; Yan, M.; Yang, C.; Chen, Z.; Lu, J.; Lu, Z. Additive manufacturing of metals: Microstructure evolution and multistage control. *J. Mater. Sci. Technol.* **2022**, *100*, 224–236. [CrossRef]
23. Anand, M.; Das, A.K. Issues in fabrication of 3D components through DMLS technique: A review. *Opt. Laser Technol.* **2021**, *139*, 106914. [CrossRef]
24. Cabrini, M.; Carrozza, A.; Lorenzi, S.; Pastore, T.; Testa, C.; Manfredi, D.; Fino, P.; Scenini, F. Influence of surface finishing and heat treatments on the corrosion resistance of LPBF-produced Ti-6Al-4V alloy for biomedical applications. *J. Mater. Process. Technol.* **2022**, *308*, 117730. [CrossRef]
25. Maimaitiyili, T.; Woracek, R.; Neikter, M.; Boin, M.; Wimpory, R.C.; Pederson, R.; Strobl, M.; Drakopoulos, M.; Schäfer, N.; Bjerkén, C. Residual Lattice Strain and Phase Distribution in Ti6Al4V Produced by Electron Beam Melting. *Materials* **2019**, *12*, 667. [CrossRef] [PubMed]
26. Available online: https://artizono.com/pl/kompleksowy-przewodnik-po-obrobce-cieplnej-stopow-tytanu/ (accessed on 12 June 2025).
27. Çevik, Z.A.; Ozsoy, K.; Erçetin, A. The Effect of Machining Process on The Pyhsical and Surface Morphology of Ti6Al4V Specimens Produced Through Powder Bed Fusion Additive Manufacturing. *Int. J. 3D Print. Technol. Digit. Ind.* **2021**, *5*, 187–194. [CrossRef]
28. *Polska Norma PN-EN ISO 25178-1:2016-08*; Specyfikacje Geometrii Wyrobów (GPS)—Struktura Geometryczna Powierzchni: Przestrzenna–Część 6: Klasyfikacja Metod Pomiaru Struktury Geometrycznej Powierzchni. Available online: https://www.iso.org/standard/46065.html (accessed on 1 April 2025).
29. *Polska Norma PN-EN ISO 10993-15*; Biologiczna Ocena Wyrobów Medycznych—Część 1: Ocena i Badanie w Procesie Zarządzania Ryzykiem. Polski Komitet Normalizacyjny: Warsaw, Poland, 2009.
30. *Polska Norma PN-EN ISO 6507-1*; Metale. Pomiar Twardości Sposobem Vickersa. Część 1 Metoda Badań. Polski Komitet Normalizacyjny: Warsaw, Poland, 2007.
31. Kajzer, W.; Szewczenko, J.; Kajzer, A.; Basiaga, M.; Kaczmarek, M.; Antonowicz, M.; Jaworska, J.; Jelonek, K.; Orchel, A.; Nowińska, K.; et al. Electrochemical and Biological Performance of Biodegradable Polymer Coatings on Ti6Al7Nb Alloy. *Materials* **2020**, *13*, 1758. [CrossRef] [PubMed]
32. Available online: https://www.metalpowder.sandvik/en/webshop/metal-powders/titanium-alloys/osprey-ti-6al-4v-grade-23/ (accessed on 1 April 2025).

33. Hucińska, J. "Metaloznastwo" Politechnika Gdańska. 1995, pp. 50–52. Available online: https://docer.pl/doc/xnx5xcn (accessed on 1 April 2025).
34. Motyka, M.; Baran-Sadleja, A.; Garcarczyk, K. Decomposition of deformed $\alpha'(\alpha'')$ martensitic phase in Ti–6Al–4V alloy. *Sci. Technol.* **2019**, *35*, 354–364. [CrossRef]
35. Lekoadi, P.; Tlotleng, M.; Annan, K.; Maledi, N.; Masina, B. Evaluation of heat treatment parameters on microstructure and hardness properties of high-speed selective laser melted Ti6Al4V. *Metals* **2021**, *11*, 255. [CrossRef]
36. Demirci, S.; Dalmiç, R.; Dikici, T.; Tünçay, M.M.; Kaya, N.; Güllüoğlu, A.N. Effect of surface modifications of additively manufactured Ti-6Al-4V alloys on apatite formation ability for biomedical applications. *J. Alloys Compd.* **2021**, *887*, 161445. [CrossRef]
37. Tardelli, J.D.C.; Valente, M.L.d.C.; Otani, L.B.; Batalha, R.L.; Alves, F.; Pereira-da-Silva, M.A.; Bagnato, V.S.; Dibb, R.G.P.; Gargarella, P.; Bolfarini, C.; et al. Analysis of physical, chemical, mechanical, and microbiological properties of Ti–35Nb–7Zr–5Ta and Ti–6Al–4V discs obtained by machining and additive manufacturing. *Ceram. Int.* **2024**, *50*, 2845–2854. [CrossRef]
38. Singh, P.K.; Kumar, S.; Jain, P.K.; Dixit, U.S. Effect of Heat Treatment on Electrochemical Behavior of Additively Manufactured Ti-6Al-4V Alloy in Ringer's Solution. *J. Mater. Eng. Perform.* **2023**, *33*, 9570–9582. [CrossRef]
39. Chávez-Díaz, M.P.; Escudero-Rincón, M.L.; Chao, J.; Arce-Estrada, E.M.; Cabrera-Sierra, R. Effect of heat treatment on the electrochemical and mechanical behavior of the Ti6Al4V alloy. *Metall. Mater. Trans. A* **2021**, *52*, 3570–3584. [CrossRef]
40. Kajzer, A.; Paszenda, Z.; Basiaga, M.; Walke, W.; Kajzer, W. Influence of surface modification on physicochemical properties of titanium used for blood contacting implants. *Eng. Biomater.* **2014**, *17*, 126.
41. Sobczak, N. Zwilżalność. struktura i właściwości granic rozdziału w układzie Al/Al_2O_3. *Composites* **2003**, *3*, 301–312.

Disclaimer/Publisher's Note: The statements, opinions and data contained in all publications are solely those of the individual author(s) and contributor(s) and not of MDPI and/or the editor(s). MDPI and/or the editor(s) disclaim responsibility for any injury to people or property resulting from any ideas, methods, instructions or products referred to in the content.